JOURNAL OF MATERIALS SCIENCE: MATERIALS IN MEDICINE 9(1998) 221–227

Dynamic fatigue and degradation in solution of hydroxyapatite ceramics

S. RAYNAUD, E. CHAMPION, D. BERNACHE-ASSOLANT, D. TETARD
Laboratoire de Matériaux Céramiques et Traitements de Surface, UPRESA CNRS 6015, 123, avenue Albert Thomas, 87060 Limoges Cedex, France

Polycrystalline hydroxyapatite was densified by hot pressing. The dissolution process in aqueous solution and the effects of environment on dynamic fatigue resistance of the resulting HAP ceramics were investigated. Pure water or Ringer's solution strongly enhances subcritical crack growth. The crack propagation exponent decreases from $22.5^{\pm 2}$ in air to $10^{\pm 4}$ in Ringer's solution for materials densified at 98% of the theoretical value. The residual porosity ratio is also very detrimental for the mechanical reliability. Both fatigue resistance and immediate fracture strength are decreased, with values of only $14^{\pm 4}$ for the propagation exponent and 40 MPa for the tensile strength (compared to 90 MPa at 98% relative density) for materials densified at 94% tested in air. The degradation in solution appears to be governed by uniform physico-chemical dissolution of crystalline HAP phase at the surface of the material. This dissolution is accompanied by a decohesion of grains located around residual pores which leads to the growth of local surface defects. © *1998 Chapman & Hall*

1. Introduction

Hydroxyapatite ($Ca_{10}(PO_4)_6OH_2$; HAP) owing to its good biocompatibility, has become a ceramic material of interest for biological implants [1–3]. As a consequence, the mechanical properties of dense HAP, immediate fracture strength and toughness, have been widely reported [4–8]. However, as for any material, the long-term application of stresses can lead to delayed fracture. This phenomenon depends on the way the load is applied, but also on the environment. Therefore, the determination of subcritical crack growth characteristics is of prime importance because it allows evaluation of the lifetime of a material under mechanical loads. In the case of HAP, it is all the more crucial that this bioceramic is known to be chemically affected when placed in a liquid or physiological environment [9–13]. But, few studies concerning the time dependence on strength are available yet [13–17]. Moreover, these investigations give very different conclusions about the fatigue behaviour of HAP. Thomas *et al.* [14] found a very strong resistance to fatigue in air with a subcritical crack propagation exponent $n = 80$. On the contrary, De With *et al.* [15] concluded that there was an important sensitivity of HAP to slow crack growth under an inert atmosphere (propagation exponent $n = 26$) with an accelerated degradation in water environment ($n = 12$). Thus, further development of reliable HAP-based materials requires a better knowledge of both mechanical fatigue behaviour and degradation in solution.

Our work consisted in determining fatigue data for hot-pressed HAP ceramics and evaluating the influence of the environment on the degradation. With this aim, dynamic fatigue experiments in air and saline solution were performed to characterize the failure process and lifetime under mechanical loads.

2. Background

Theoretical and experimental approaches to fatigue failure in brittle (linear-elastic) materials have been widely reported in the literature [18–22]. It is analysed in terms of subcritical crack growth which is generally described through the power-law relationship

$$V = \frac{da}{dt} = A K_I^n \tag{1}$$

where V is the crack velocity, a the crack length, K_I the stress intensity factor at the crack tip, A a constant and n the propagation exponent. This exponent, n, is considered to be a characteristic of the resistance to mechanical fatigue of a material under a given environment.

A typical (K_I, V) curve, shown in Fig. 1, can be divided into three regions depending on material and environmental factors:

region I, in which crack motion is assumed to be controlled by stress-enhanced chemical reaction at the crack tip;

region II, in which crack velocity does not depend strongly on the stress intensity factor ($n = 0$). Crack motion is controlled by the diffusion rate of corrosive species to the crack tip;

region III, in which the crack velocity increases rapidly and K_I reaches the critical stress intensity factor, K_{Ic}. The crack motion is governed by brittle

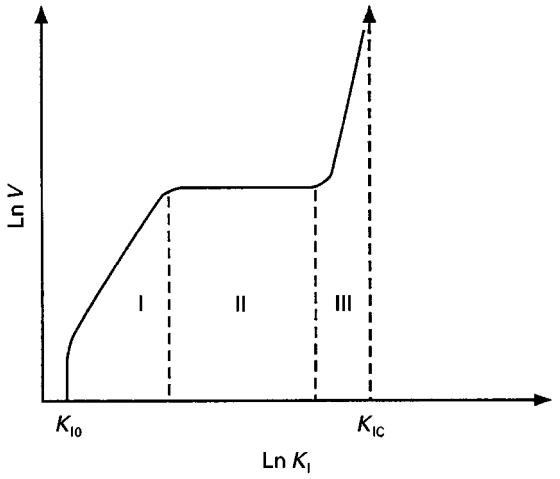

Figure 1 Typical plot of slow crack growth versus stress intensity factor.

fracture mechanisms, associated with a high exponent of crack propagation.

The stress intensity factor, K_I, is also defined from crack length and stress by the equation

$$K_I = Y\sigma a^{1/2} \quad (2)$$

From the combination of Equations 1 and 2, several formulations have been developed to yield more precisely the fatigue behaviour of a material in correlation with experimental methods. In this field, two testing techniques, based on fracture strength measurements, appear advantageous [23–25].

(i) Dynamic fatigue at constant stressing rate. The fracture strength depends on the stressing rate according to the relation

$$\sigma_f^{n+1} = B(n+1)\sigma_i^{n-2}\dot{\sigma} \quad (3)$$

where σ_f is the fracture strength, B a constant, σ_i the inert fast fracture strength, and $\dot{\sigma}$ the stressing rate. A more convenient formulation of this equation is

$$\ln\sigma_f = \frac{1}{n+1}\ln[B(n+1)\sigma_i^{n-2}] + \frac{1}{n+1}\ln\dot{\sigma} \quad (4)$$

Thus, the measurement of fracture strength at different stressing rates allows the determination of the propagation exponent n from the slope of the straight line on the graph $\ln\sigma_f = F(\ln\dot{\sigma})$.

(ii) Static fatigue at constant applied load. In this case, the time-to-failure or lifetime under a constant applied load is defined by the relationship

$$t_f = B\sigma_i^{n-2}\sigma_a^{-n} \quad (5)$$

where t_f is time to failure, and σ_a the applied stress. As previously, the measurement of the time-to-failure at different applied loads allows calculation of the propagation exponent, according to the relation

$$\ln t_f = \ln B\sigma_i^{n-2} - n\ln\sigma_a \quad (6)$$

In our study, dynamic fatigue experiments were performed to calculate the crack propagation exponent. Then the static fatigue Equation 6 was applied from the results obtained in dynamic fatigue to simulate the lifetime of the material.

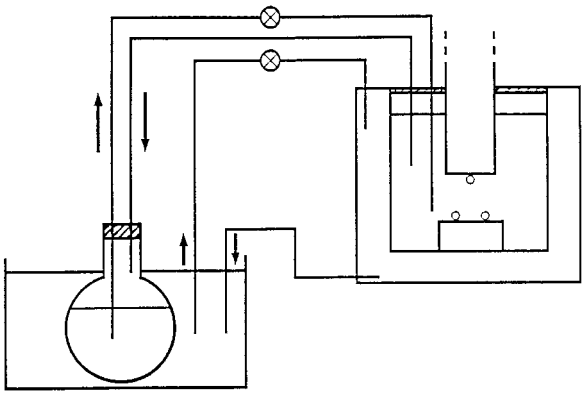

Figure 2 Schematic representation of the device used for mechanical testing in a controlled liquid environment.

3. Experimental procedure

A commercial stoichiometric hydroxyapatite powder (Bioland) was used in this study. Its main characteristics and its preparation are described in a previous paper [7]. This powder was hot pressed under a constant compressive stress of 10 MPa, either at 1165 °C for 1 h or at 1100 °C for 30 min. Heating and cooling rates were 15 °C min^{-1} and 10 °C min^{-1}, respectively. The resulting HAP ceramics had a relative density, measured using Archimedes' method in water, of $98.1 \pm 0.1\%$ after hot pressing at 1165 °C and $94.0 \pm 0.1\%$ (hot pressing at 1100 °C) of the theoretical value which was assumed to be 3.156 g cm^{-3}.

Sintered blocks were cut into bars of $4 \times 3 \times 25$ mm^3 using a diamond saw and each bar was polished with 3 μm diamond paste. Quasi-static, or immediate, fracture strength in air was determined by three-point bending with a 16 mm span and a crosshead speed of 0.2 mm min^{-1} .

Sample surface examinations were performed by scanning electron microscopy (SEM). The microstructure of hot-pressed materials was revealed from mirror-polished surfaces. These surfaces were thermally etched by heating the samples for 3 min at a temperature of 30 °C below the sintering temperature.

Two types of experiments were performed to characterize the behaviour of HAP materials in solution.

(i) Ageing of HAP samples in solutions. The dissolution of HAP ceramics was investigated either in pure water or Ringer's solution on mirror-polished samples of about 500 mg immersed in flasks containing 200 ml solution at 37 °C. The degradation of the samples was evaluated by measurements of surface roughness (surface profiler Dektak IIA slow technology), weight of the samples (measured with standard deviation of $\pm 5 \times 10^{-5}$ g) and pH of the solution for immersion times ranging from 1 d to 3 wk.

(ii) Mechanical testing of HAP samples by dynamic fatigue in solution. In this case, a device shown schematically in Fig. 2, was included to determine the resistance to slow crack growth in a controlled liquid environment. The testing solution was circulated between a flask and a mechanical testing cell. To ensure a constant temperature of the solution during the whole duration of an experiment, the flask containing

TABLE I Composition of solutions (main ions) [27]

	Simplified Ringer's solution	Extra-cellular fluid
Na^+ (mmol l^{-1})	147	142
K^+ (mmol l^{-1})	4	5
Ca^{2+} (mmol l^{-1})	3	2.5
Mg^{2+} (mmol l^{-1})	—	1.5
Cl^- (mmol l^{-1})	157	103

it was immersed in a thermostated bath, the water of which also circulated inside the cell walls.

For dynamic fatigue tests, the crosshead speed varied in the range 3×10^{-3}–2 mm min^{-1}. This corresponded to constant stressing rates ranging from 3×10^{-2}–20 MPa s^{-1}. Dynamic fatigue experiments were performed either in air or liquid solution at 37 °C. As the determination of fracture strength measured by three-point bending can be biased by the location of the flaw which initiates crack propagation, an artificial defect was generated on the surface of the samples by Vickers indentation [26] under a 4.9 N load prior to testing in solution.

Different solutions are commonly used to study the stability of biomaterials [27]. In this work, a Ringer's solution was used; its composition compared to the extra-cellular fluid is given in Table I. The components used for its preparation were high-purity NaCl, KCl and $CaCl_2 \cdot 2H_2O$ chemical grades (Merck).

4. Results and discussion

4.1. Degradation in solution

Table II summarizes the changes in pH of water or Ringer's solution versus immersion time of HAP samples densified at 94% and 98%. A decrease of the pH of the solutions was observed. This decrease was more important in water (− 1.2 pH unit after 3 wk) than in Ringer's solution (− 0.5 pH unit after the same duration) but the changes were similar whatever the densification ratio of the samples. The decrease in pH was associated with a weight loss of the samples related to dissolution mechanisms of HAP. For all the experiments, the total weight loss remained very low and reached a maximum of only about 0.2% after 3 wk immersion. The difference in densification ratio of the initial samples did not seem to modify this result. This indicated that globally there was no significant influence of the residual porosity on the degradation phenomenon.

Considering the dissolution equilibrium of HAP:

$$Ca_{10}(PO_4)_6(OH)_2 \rightleftharpoons 10\,Ca^{2+} + 6\,PO_4^{3-} + 2OH^- \quad (7)$$

with $K_s = 5.42 \times 10^{-121}$ [28], the solubility of HAP would be around 3×10^{-5} g L^{-1} in water and about 3×10^{-10} g L^{-1} in Ringer's solution. The pH of the solutions should increase, whereas a decrease was registered. A similar evolution in pH values has already been reported in the literature [10] and was attributed to the formation of chemical species such as

TABLE II pH of the solutions versus immersion time for HAP materials

Duration	Sample (94%)		Sample (98%)	
	Water	Ringer's solution	Water	Ringer's solution
Initial	7.95	6.09	8.00	6.15
24 h	7.49	5.91	7.22	6.02
72 h	6.85	5.87	6.99	5.96
1 wk	6.83	5.64	6.91	5.93
2 wk	6.85	5.60	6.87	5.82
3 wk	6.81	5.54	6.82	5.64

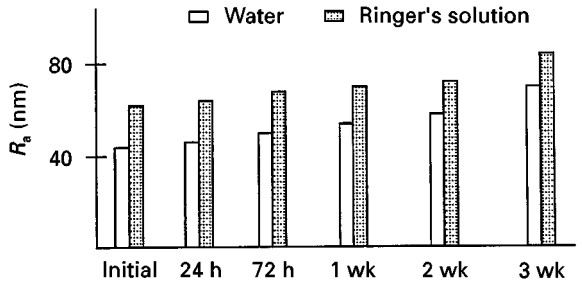

Figure 3 Surface roughness versus immersion time for HAP densified at 98%.

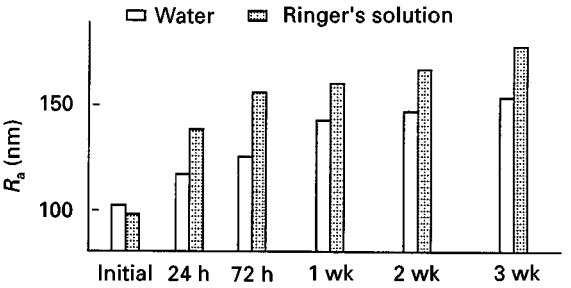

Figure 4 Surface roughness versus immersion time for HAP densified at 94%.

$CaOH^+$, $H_2PO_4^-$ or $CaH_2PO_4^+$. This implies that several other chemical reactions between ions resulting from HAP dissolution occur simultaneously, either in the solution or on the surface of the material. Consequently, the calculated values should represent an underestimation of the real solubility of HAP. Moreover, owing to the different reactions which may occur in this case, it appears difficult to calculate the solubility value with a satisfactory accuracy. Nevertheless, the weight loss measured on HAP samples, which was about 5×10^{-3} g L^{-1} after 3 wk immersion, must be too high to be caused by the single uniform dissolution of HAP material, as will be confirmed below.

Figs 3 and 4 show the evolution of the average roughness R_a, of sample surfaces after different durations of immersion in water and Ringer's solution. For HAP densified at 98%, the initial values of R_a ranged from 45–60 nm depending on the samples, and was close to 100 nm for samples densified at 94%. The differences between these values can be explained by

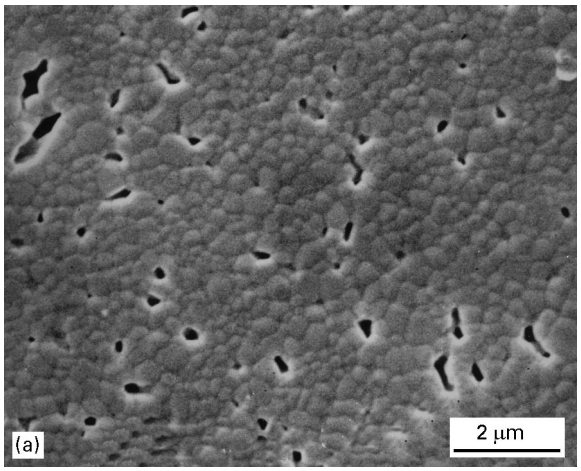

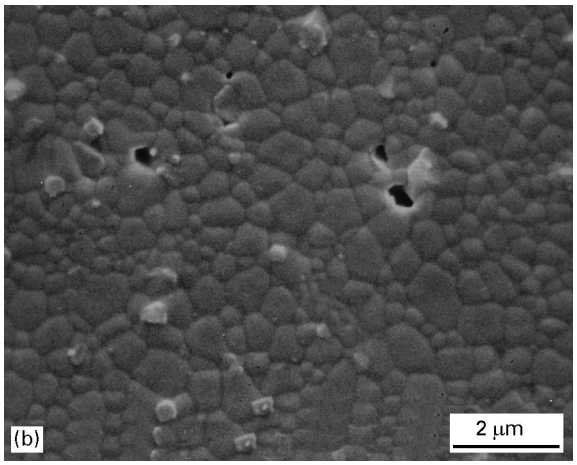

Figure 5 Scanning electron micrographs of the surface of HAP materials: (a) densified at 94%, (b) densified at 98%.

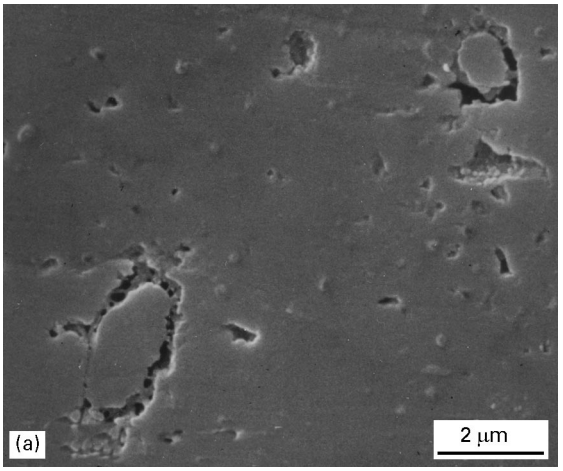

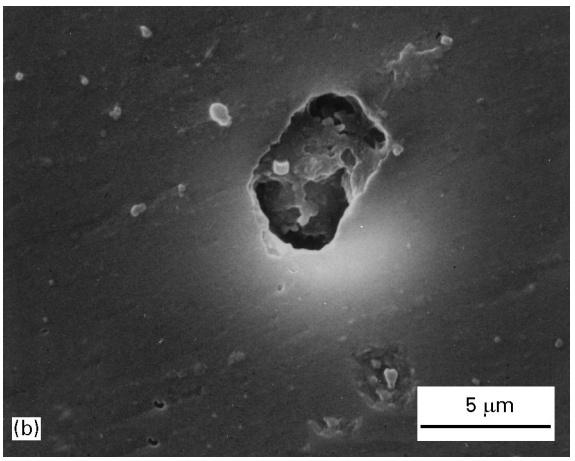

Figure 6 Scanning electron micrographs of materials surfaces after 3 wk immersion in Ringer's solution: (a) HAP densified at 94%, (b) HAP densified at 98%.

the presence of more or less numerous residual pores at the surface of materials, as shown in Fig. 5.

Whatever the densification ratio, the average roughness increased as the immersion time was increased. This increase was less important when the samples were immersed in water than in Ringer's solution. Thus, the presence of ionic species in the solution enhances the degradation rate. For HAP materials densified at 94%, a doubling of R_a value was noticed, increasing from 100 nm at the initial time to 200 nm after 3 wk of immersion in Ringer's solution. This augmentation of average surface roughness was less important in the case of samples densified at 98%.

Scanning electron micrographs of HAP surfaces after 3 wk of immersion in Ringer's solution are given in Fig. 6. Compared with the initial surfaces, they show that the degradation of the material surface was not uniform. Only some regions appeared strongly degraded with the formation of rings like grooves (Fig. 6a) the dimensions of which correspond to the grains size. To a lesser extent, some cavities as large as 5 μm were also observed (Fig. 6b). Degraded regions were similar but more numerous in the case of HAP densified at 94% than for materials densified at 98%. In both cases, dense or pore-free regions did not seem to be degraded. From these microstructural observations, it can be assessed that the degraded regions are more particularly located around residual pores which were present at the surface of the initial material. This indicates that the dissolution of HAP is accompanied by the decohesion of some grains. This decohesion explains why the weight losses registered were more important than expected by a single dissolution mechanism.

Different interpretations can be found to explain the degradation mechanisms of calcium phosphate materials in liquid environments. For HAP ceramics, they are based on the hypothesis of two different dissolution processes.

(i) A decohesion of HAP grains, as observed by Nonami and Wakai [17], governed by a higher solubility of grain boundaries, the chemical composition of which after sintering (calcium deficient or amorphous phases) differs from that of the grains themselves. Although decohesion occurred during degradation, this hypothesis of a preferential dissolution of grain boundaries does not allow the observed behaviour to be totally explained. The presence of a calcium-deficient phase at grain boundaries, more soluble than stoichiometric HAP, also leads to the revelation of the microstructure by chemical etching of grain boundaries at the surface of the material after immersion. This phenomenon was not observed in our experiments.

Moreover, microstructural analyses of HAP materials similar to that used for our experiments, confirmed the presence of only crystalline HAP either in grains or grain boundaries [29];

(ii) A uniform physicochemical dissolution of grains, depending on the solubility product of HAP [10, 13], and which seems consistent with our results. For our materials, it can be hypothesized that the degradation proceeds through HAP surface dissolution. This dissolution would induce a diminution of cohesion between grains around residual pores. This would lead to a preferential decohesion of grains located around these pores. Then, the decohesion could progress gradually inside the material and cause the removal of small pieces of materials made up of several grains, thus explaining the presence of cavities. This could also explain why dense regions of the surface do not appear degraded, even though the surface dissolves.

4.2. Dynamic fatigue

A typical plot of fracture strength versus stressing rate is shown in Fig. 7. The slope of a plot of $\ln \sigma_f$ and $\ln \dot{\sigma}$, determined from the least squares line, allows the crack propagation exponent, n, to be calculated. However, as demonstrated by Ritter *et al.* [30], care must be taken because of important uncertainties which may arise from statistical analysis of the crack propagation exponent. Poor reproducibility may be obtained, depending on both experimental procedure and materials characteristics such as Weibull modulus or fatigue resistance. Consequently, F-distribution was used to evaluate the validity of linear regressions for each plot and t-distribution was used to estimate the standard deviation of the calculated values of n. The resulting equations and confidence levels of linear regressions for materials densified at 94% and 98%, tested either in air or Ringer's solution, are given in Table III.

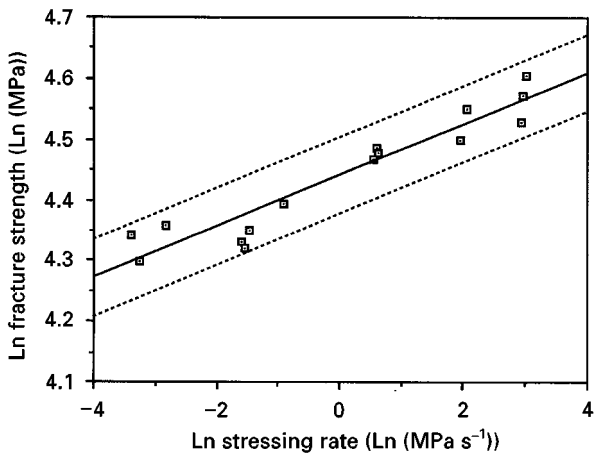

Figure 7 Fracture strength versus stressing rate in air for HAP densified at 98%: (...) the 95% confidence level.

From this method, values of $n = 22.5 \pm 2$ and 14 ± 4 were obtained for HAP ceramics tested in ambient air and densified at 98% and 94% theoretical density, respectively. The propagation exponent $n = 10 \pm 2$ for materials at 98% relative density tested in Ringer's solution. No value of n is given for samples densified at 94% tested in solution, because very low values of fracture strength were measured which were associated with wide standard deviations. This resulted in a low confidence level of the linear regression (about 75%) and therefore to a non-significant value of n.

Although an augmentation of 4% of the residual porosity did not modify the behaviour of the materials when placed in solution, as shown in the previous section, it has an important influence on the mechanical characteristics of HAP. In air, both fracture and resistance to subcritical crack growth decrease as the volume fraction of residual pores increases. Values of 90 MPa and 22.5 were obtained at 98% of relative density for immediate fracture strength and crack propagation exponent, respectively, whereas they were only 40 MPa and 14 at 94%. In the same way, the liquid environment induces a drastic drop in the resistance to fatigue, the propagation exponent decreasing from 22.5 in air to 10 in Ringer's solution for HAP ceramics densified at 98%.

These results on mechanical fatigue characteristics can be clearly illustrated by the evaluation of time-to-failure under a fixed load. Indeed, dynamic fatigue experiments allow us to predict an estimation of the lifetime of a material. The constant A_0 of Equation 4 $\ln \sigma_f = A_0 + A_1 \ln \dot{\sigma}$ is equal to $(n+1)^{-1} \times \ln[B(n+1)\sigma_i^{n-2}]$, that is

$$\ln[B\sigma_i^{n-2}] = A_0(n+1) - \ln(n+1), \qquad (8)$$

Thus, Equation 6 can be rewritten as follows

$$\ln t_f = A_0(n+1) - \ln(n+1) - n \ln \sigma_a \qquad (9)$$

The plots of $\ln t_f$ versus $\ln \sigma_a$, for simulated values of σ_a and for the values of the constants A_0 and n derived from the linear regressions of dynamic fatigue data, are given in Fig. 8. From these plots it can be seen that the lifetime under mechanical loads is much shorter when the material is subjected to a liquid environment. For example, the lifetime would be about 2 y in air for HAP densified at 98% and loaded at 45% of its immediate fracture strength, but only 100 h in solution under a load corresponding to a tensile stress of

TABLE III Statistical analysis of dynamic fatigue plots

Testing conditions	Linear regression	r^2	Confidence level (%)
HAP 98% in air	$\mathrm{Ln}\sigma = 4.43 + 4.23 \times 10^{-2} \ln \dot{\sigma}$	0.910	95
HAP 98% in solution	$\mathrm{Ln}\sigma = 4.48 + 9.05 \times 10^{-2} \ln \dot{\sigma}$	0.812	99
HAP 94% in air	$\mathrm{Ln}\sigma = 4.04 + 6.59 \times 10^{-2} \ln \dot{\sigma}$	0.587	99
HAP 94% in solution	$\mathrm{Ln}\sigma = 3.63 + 6.73 \times 10^{-3} \ln \dot{\sigma}$	0.065	75

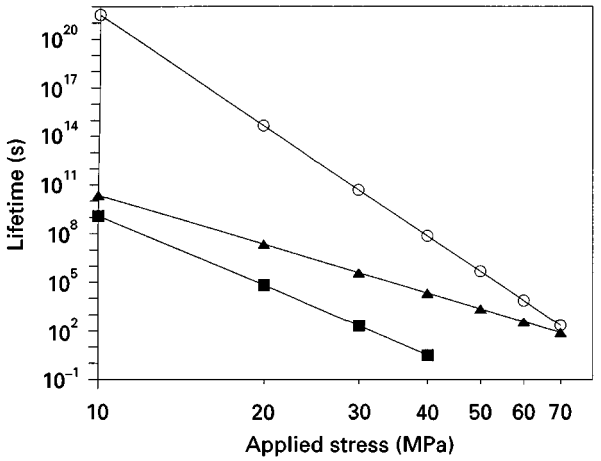

Figure 8 Simulated plots of lifetime versus applied load: (○) HAP 98% in air, (▲) HAP 98% Ringer's solution, (■) HAP 94% in air.

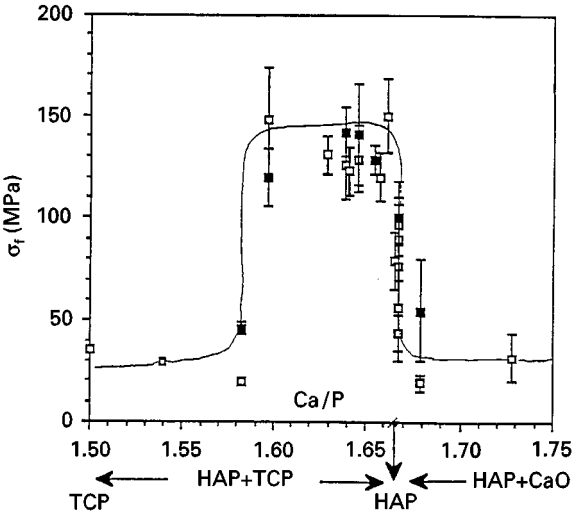

Figure 9 Fracture strength of calcium phosphates versus Ca/P atomic ratio, from [31]. (■) 1150 °C, and (□) 1250 °C.

30 MPa (i.e. loaded at around 30% of its fracture strength). It can be noted that the decrease of mechanical characteristics might not result from surface defects created by grain decohesion during immersion because indentation cracks were initially produced to prevent the contribution of surface defects on the measurements. Moreover, dynamic fatigue tests did not exceed 2 h, which might be thought to be too short for the grain decohesion process to occur. This indicates that stress-enhanced chemical reaction proceeds at the crack tip, resulting in a very low resistance to subcritical crack propagation and, consequently, to a poor mechanical reliability of HAP. Therefore, it can be reasonably thought that uniform dissolution of HAP at the crack tip should be responsible for the augmentation of subcritical crack growth.

Considering the literature data, the values of crack propagation exponents determined for our HAP ceramics can be compared to those found by de With *et al.* [15] or de Groot [13], though environmental conditions of the tests may be somewhat different. On the other hand, they are considerably inferior to that given by Thomas *et al.* ($n = 80$ in an air atmosphere) [14]. Such a different behaviour might be explained by a contribution of brittle fracture mechanisms (region III of subcritical crack growth) which can be effective in dynamic fatigue experiments realized at elevated stressing rates and can result in higher average values of the crack propagation exponent. Nevertheless, care should be taken on comparisons concerning the mechanical behaviour of different HAP ceramics. Great variations of fracture strength versus Ca/P atomic ratio of calcium phosphates, given in Fig. 9, have been reported by Royer *et al.* [31]. At the stoichiometric value of Ca/P = 5/3, an important drop in the fracture strength occurred, showing that very different results can be obtained for stoichiometric HAP. Thus, even very small changes in the Ca/P ratio around the stoichiometry can lead to very different mechanical characteristics. This phenomenon can be illustrated by comparing the results obtained in a previous study [17], Fig. 10 gives the evolution of

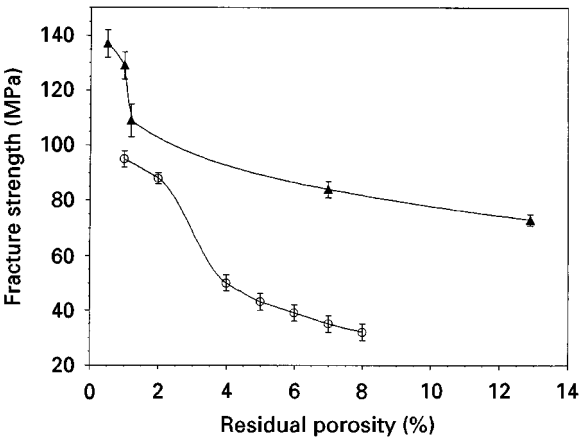

Figure 10 Fracture strength of HAP materials versus residual porosity ratio: (○) present batch of HAP powder, (▲) previous batch, from [7].

fracture strength for HAP ceramics obtained from another batch of powder and produced using the same processing technique as that used in the present work. Evidence exists for very different mechanical characteristics, the present HAP materials being less resistant than the previous ones, whereas no chemical change was observed on X-ray diffraction patterns of the initial and sintered powders. Finally, the fatigue resistance of HAP ceramics should be affected in a similar way by this phenomenon, which could also explain the differences in the literature data concerning crack-exponent parameters for HAP.

5. Conclusion

This study has shown that pure HAP ceramics degrade in a liquid environment by surface dissolution and further grain decohesion around residual pores. This results in the formation of surface defects of increasing dimensions. From a mechanical point of

view, the behaviour of HAP materials depends strongly on the presence of residual pores. They constitute critical defects which lead to an important reduction of the resistance of fatigue in air. Additionally, subcritical crack growth is enhanced by HAP dissolution at the crack tip. Finally, HAP ceramics are very sensitive to crack propagation. Composite technology appears to be a requisite means of improving the mechanical reliability of the material and to extend its potential applications. Promising results have already been obtained on HAP-based composites to improve the resistance to crack propagation [32]. In the light of the present study, it is expected that further improvements in the resistance to slow crack growth will also be reached, provided that a good control of the chemical composition and microstructural design of the HAP matrix is obtained to prevent the detrimental effect of grain decohesion on the mechanical behaviour in a liquid environment.

References

1. U. HEISE, J. F. OSBORN and F. DUWE *Int. Orthopaed.* **14** (1990) 329.
2. H. OONISHI, *Biomaterials* **12** (1991) 171.
3. L. L. HENCH, *J Am. Ceram. Soc* **74** (1991) 1487.
4. M. JARCHO, C. H. BOLEN, M. B. THOMAS, J. BOBICK, J. F. KAY and R. H. DOREMUS, *J Mater. Sci.* **11** (1976) 2027.
5. M. AKAO, H. AOKI and K. KATO, *ibid.* **16** (1981) 809.
6. Y. HIRAYAMA, H. IKATA, H. AKIYMA, K, NAGAMURA, S. OJIMA and M. KAWAKAMI, in "Sintering 87", edited by S. Somiya, M. Shimasa, M. Yoshimura and M. Watanabe (Elsevier, New York, 1987) p. 1332.
7. R. HALOUANI, D. BERNACHE-ASSOLLANT, E. CHAMPION and A. ABABOU, *J. Mater. Sci. Mater. Med.* **5** (1994) 563.
8. P. VAN LANDUYT, F. LI, J. P. KEUSTERMANS, J. M. STREYDIO, F. DELANNAY and E. MUNTING, *ibid.* **6** (1995) 8.
9. F. BISSON, P. GOHAR and D. BERNACHE-ASSOLLANT, in "Euro-ceramics", Vol. 3, edited by G. De With, R. A. Terpstra, R. Metselaar (Elsevier Applied Science, London, 1989) p. 3.58.
10. P. DUCHERYNE, C. S. KIM and S. R. POLLAK, *J. Biomed. Mater. Res.* **26** (1992) 147.
11. P. DUCHEYNE, S. RADIN and L. KING, *ibid.* **27** (1993) 25.
12. C. A. Van BLITTERSWIJK, J. J. GROTE, K. de GROOT, W. T. DAEMS and W. KUYPERS, *J Biomed. Mater. Res.* **20** (1986) 989.
13. K. de GROOT, in "Bioceramics", edited by P. Ducheyne and J. Lemons (Annals New York Academy of Science, NY, 1988) p. 227.
14. M. B. THOMAS, R. H. DOREMUS, M. JARCHO and R. L. SALSBURY, *J. Mater. Sci.* **15** (1980) 891.
15. G. de WITH, H. J. A. VAN DIJK, N. HATTU and K. PRIJS, *ibid.* **16** (1981) 1592.
16. S. M. BARINOV and V. Y. SHEVCHENKO, *J. Mater. Sci. Lett.* **14** (1995) 582.
17. T. NONAMI and F. WAKAI, *J. Ceram. Soc. Jpn* **103** (1995) 648.
18. A. G. EVANS and H. JOHNSON, *J. Mater. Sci.* **10** (1975) 214.
19. B. R. LAWN, D. B. MARSHALL, G. R. ANSTIS and T. P. DABBS, *ibid.* **16** (1981) 2846.
20. B. J. PLETKA and S. M. WIEDERHORN, *ibid.* **17** (1982) 1247.
21. S. M. WIEDERHORN, S. W. FREIMAN, E. R. FULLER Jr and C. J. SIMMONS, *ibid.* **17** (1982) 3460.
22. J. C. GLANDUS, *ibid.* **26** (1991) 4667.
23. A. G. EVANS, *Int. J. Fract.* **10** (1974) 251.
24. J. E. RITTER Jr and J. N. HUMENIK, *J. Mater. Sci.* **14** (1979) 626.
25. T. FETT and D. MUNZ, *J. Eur. Ceram. Soc.* **6** (1990) 67.
26. C. B., PONTON and R. D. RAWLINGS, *Mater. Sci. Technol.* **5** (1989) 865.
27. M. A. BARBOSA, in "Biomaterials degradation", edited by M. A. Barbosa (Elsevier Science, Amsterdam, 1991) p. 227.
28. E. C. MORENO, M. KRESAK and R. T. ZAHRADNIK, *Caries Res.* **11** (1977) 142.
29. H. J. KLEEBE, E. F. BRES, D. BERNACHE-ASSOLLANT and G. ZIEGLER, *J. Am. Ceram. Soc.*, **80** (1997) 37.
30. J. E. RITTER Jr, N. BANDYOPADHYAY and K. JAKUS, *ibid.* **62** (1979) 542.
31. A. ROYER, J. C. VIGUIE, M. HEUGHEBAERT and J. C. HEUGHEBAERT, *J. Mater. Sci. Mater. Med.* **4** (1993) 76.
32. S. GAUTIER, E. CHAMPION and D. BERNACHE-ASSOLLANT, *J. Eur. Ceram. Soc.*, accepted for publication.

Received 1 April
and accepted 22 May 1997